Additively Manufactured Stacked Refrigerant-to-Water Condenser

Mohammad Reza Shaeri[1], Sajjad Bigham[2], Vivek Mohan[2], Maksym Demydovych[1]
[1] *Advanced Cooling Technologies, Inc., Lancaster, PA 17601*
[2] *Department of Mechanical and Aerospace Engineering, North Carolina State University, Raleigh, NC 27695*
MohammadReza.Shaeri@1-act.com

***Abstract*—Filmwise condensation (FWC) is the dominant condensation mode in industrial systems due to the high surface energy of commonly used metals. Enhancing FWC can reduce the size, weight, and power (SWaP) of thermal management hardware. However, due to the extreme wetting characteristics of low-surface-tension fluids, enhancing FWC of these fluids remains challenging. For the first time, this study presents a scaled-up metallic 3D-printed liquid-cooled condenser to enhance FWC of refrigerants. Water is used as the coolant to condense the vapor of refrigerant R134a. The water side of the condenser incorporates cylindrical pin fins. The condenser's innovation lies in its refrigerant side, which includes capillary channels (wicks) with a two-dimensional gradient pore size distribution (2D-GPSD). This gradient wick design partially decouples wick capillary pressure, wick permeability, and effective thermal conductivity of the wick-condensate, thereby enhancing capillary-driven condensation. The condenser was made of stainless steel and comprised five refrigerant layers, each positioned between two of the six water layers. Experiments were conducted across various inlet water temperatures, refrigerant flow rates, and two operating orientations: horizontal and gravity-assisted orientations. The latter configuration aids in removing the liquid film from the wick, thereby enhancing the FWC. Operating in the gravity-assisted orientation increased the condensation heat flux by over 43% compared to horizontal operation and resulted in significantly higher condensate formation. With further optimization, the present condenser has significant potential to reduce the SWaP of two-phase thermal management systems.**

Keywords— Thermal management system; Liquid-cooled condenser; Filmwise condensation; Gradient wick structure; Additive manufacturing.

I. INTRODUCTION

The increasing power of electronic devices, combined with their ongoing miniaturization, has led to rapidly growing heat fluxes, resulting in numerous local hotspots that thermally limit device operation [1,2]. To maintain performance, reliability, and extend the lifespan of electronic devices, the development of effective cooling technologies is urgently needed. Rising heat fluxes have shifted focus to two-phase thermal management systems like flow boiling, which are highly effective due to their superior heat transfer coefficient over single-phase methods [3]. In two-phase systems, heat is initially removed from heat-generating devices through boiling and then released to the environment via condensation, requiring compact designs to meet strict volume and weight constraints in high-heat-flux applications [4]. The majority of research on two-phase thermal management has focused on boiling and evaporation, whereas condensation, a crucial aspect of two-phase systems, has received relatively less attention [5]. While commercial condensers can meet cooling requirements, they are often bulky and inefficient [6]. As a result, developing compact and efficient condensers by enhancing condensation heat transfer is crucial to minimizing the Size, Weight, and Power (SWaP) of thermal management systems.

Condensation typically occurs in two main forms: filmwise condensation (FWC) and dropwise condensation (DWC) [7]. FWC is characterized by the formation of a liquid film on the surface, which adds an additional thermal resistance [8]. In DWC, small droplets form at specific nucleation sites and grow through direct condensation and coalescence. Once they reach a critical size, they begin to move across the surface, clearing the surface for new nucleation sites to form [9]. Although DWC is a preferred mode of condensation with a heat transfer coefficient up to one order of magnitude higher than FWC, promoting its use in industrial applications has remained a challenge [10,11]. The condensation mode is mainly influenced by the properties of the condensing surface, the thermophysical characteristics of the condensate, and the operating conditions [12]. It is widely accepted that hydrophobic surfaces promote DWC, while hydrophilic surfaces facilitate FWC [13,14]. FWC is the dominant mode of condensation in industrial applications due to the high surface energy of commonly used metals. Functional coatings offer a way to decrease the high surface free energy associated with metals, thereby enhancing DWC. However, the primary challenge for industrial applications lies in ensuring the durability of these coatings in harsh environments, characterized by high temperatures, heat flux, and vapor velocity [15].

In addition, greater challenges arise when enhancing the condensation of low-surface-tension fluids such as hydrocarbons, alcohols, and refrigerants. These fluids are widely used in a variety of industrial applications, such as chemical plants, natural gas production, biomass combustion,

food industry, building energy technology, etc. [16]. Maintaining stable DWC of low-surface-tension fluids remains challenging [17], as advanced condenser materials have surface energies comparable to the surface tension of these fluids, leading to FWC [18]. As a result, effective approaches to improving the compactness of industrial condensers should focus on techniques that enhance FWC.

In this study, we leverage the advantages of wick structures to develop a compact condenser that enhances FWC of refrigerants. Wick structures enhance FWC due to (i) larger condensation areas compared to a plain surface, and (ii) a lower thermal resistance of condensate-wick compared to that of a liquid film on a plain surface. Some previous research on using wick structures to enhance FWC can be found in [19–21]. However, fabricating the proposed wick structures using traditional techniques would be extremely challenging. Most efforts to enhance heat transfer in heat exchangers have focused on adding internal structures within the flow passage. However, these efforts have primarily targeted simple structures rather than complex ones, mainly due to the manufacturing limitations of traditional techniques [22]. Consequently, fabricating hydrothermally optimized components derived from simulations has remained a significant challenge using conventional manufacturing techniques. However, advancements in metal additive manufacturing (AM) have made it possible to fabricate complex heat exchangers featuring intricate flow designs. Unlike traditional manufacturing methods, AM allows for the creation of thinner walls, which helps to decrease both weight and thermal resistance. AM, also known as 3D printing, has become a vital aspect of advanced manufacturing technologies due to its exceptional versatility in fabricating intricate geometries and tailored parts directly from digital models [23]. Recent advancements in developing 3D-printed two-phase cold plates integrated with wick structures can be found in [24–28]. Specifically, we have recently demonstrated the effectiveness of a novel 3D-printed wicked condenser made of copper in enhancing the FWC of HFE-7100, a low-surface-tension fluid [29].

For the first time, this study presents a scaled-up 3D-printed liquid-cooled condenser to enhance FWC of low-surface-tension fluids. Water is used as the coolant to condense the vapor of refrigerant R134a. The novelty of the condenser lies in its refrigerant side, which incorporates wick structures with gradient pore size distributions in two dimensions. This condenser has significant potential to reduce the SWaP of thermal management hardware through the optimization of features on both the refrigerant and coolant sides.

II. Experiment

This section presents the fabrication process of the condenser prototype, the experimental procedure, and the data reduction analysis.

A. 3D Printing of Condenser

The heat exchanger design in this study consists of two sections: the condenser and the coolant side, referred to as the refrigerant side and water side, respectively, throughout this paper. Both sections are located opposite each other and are separated by a thin wall. The refrigerant vapor enters the condenser and is condensed by the cooling provided by the circulating water on the coolant side. Fig. 1 shows the 3D-printed single-layer condenser prior to welding the inlet and outlet manifolds. This condenser comprises one layer of refrigerant section and one layer of coolant section. The inlet and outlet ports have a diameter of 6.35 mm. The condenser was manufactured using a GE Concept Laser 3D printer with 17-4PH stainless steel. The purpose of fabricating the condenser with a trapezoidal footprint is to reduce its weight while maintaining high thermal performance. However, the condenser can be manufactured in other geometries, such as a rectangular footprint. The condenser includes separate inlet and outlet manifolds for the refrigerant flow, as well as distinct manifolds for the coolant. This design allows for the study of both cocurrent flow and counter-current flow configurations, corresponding to the same and opposite flow direction of refrigerant and coolant, respectively. In this study, the condenser operates in a cocurrent flow configuration. The wall separating the coolant and refrigerant sides is 1.6 mm thick.

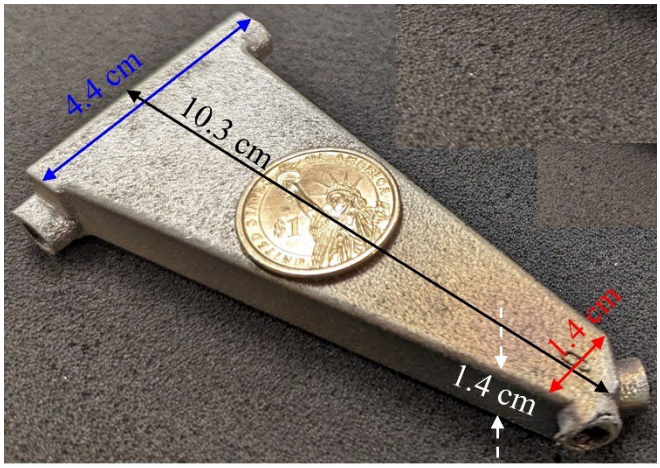

Fig. 1. 3D-printed single-layer condenser with one refrigerant layer and one coolant layer, made of stainless steel.

The CAD model of the coolant side (i.e., the water side) is illustrated in Fig. 2. The coolant side consists of cylindrical pin fins with a diameter of 1.5 mm, a height of 4.76 mm, and a center-to-center spacing of 3.5 mm.

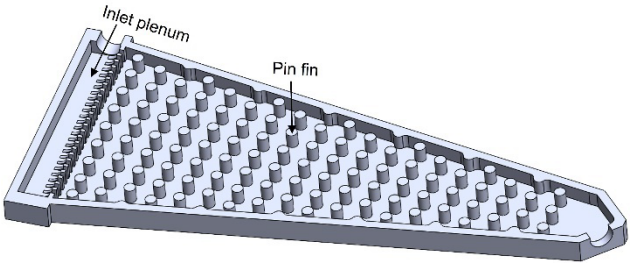

Fig. 2. CAD model of the coolant side (i.e., water side).

The refrigerant side consists of two alternating converging capillary structures (i.e., wicks), three diverging empty spaces,

and an outlet wick. Each wick is surrounded by two empty spaces. The outlet wick is a capillary structure that connects all individual wicks to (i) avoid discontinuity in the capillary pressure and liquid meniscus at the outlet of the condenser, and (ii) prevent by-pass of the refrigerant vapor.

The novelty of the presented condenser lies in the refrigerant side, which features gradient lattice wick structures with decreasing pore sizes from the inlet to the outlet of condenser, as well as decreasing pore sizes from the center of wick to the edge of the wick. This capillary structure is referred to as a two-dimensional gradient pore size distribution (2D-GPSD) wick. The design rationale for these wicks, along with their merits, will be discussed in a separate section. The wick structure has a height of 4.76 mm and a wall thickness of 300 µm. To visualize the interior of the condenser, an X-ray image of a single-layer condenser is shown in Fig. 3. Pin fins are visible on the water side, while gradient wicks are observed on the refrigerant side of the condenser.

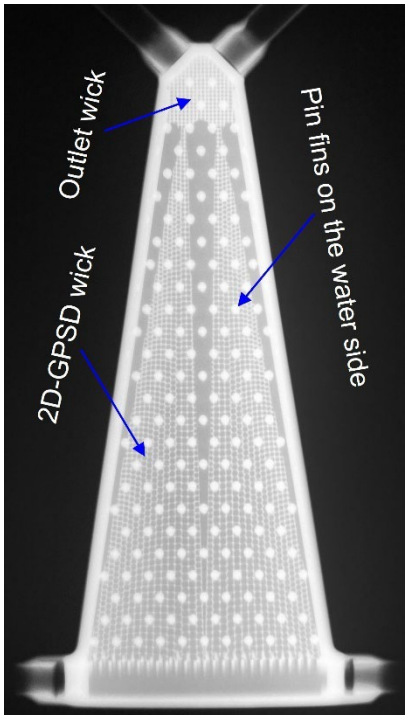

Fig. 3. X-ray image of the condenser showing 2D-GPSD wicks on the refrigerant side, and cylindrical pin fins on the water side.

At the inlet of the condenser, the refrigerant vapor flows through the capillary channels with large pore sizes. At each capillary channel, the condensation occurs inside the wicks; then, the condensate is drawn laterally to two empty spaces by the wick capillary pressure (P_{cap}). That part of vapor flowing inside the empty spaces is also condensed on the vertical walls of the capillary channels and the horizontal plain surface. By increasing the distance from the inlet, the amount of condensate increases inside the condenser such that close to the outlet, the condenser is filled with pure liquid. Then, the liquid is wicked through the outlet wick and is pumped outside the condenser.

A stacked condenser design, which is the main design of the present study, represents a scaled-up condenser with multiple refrigerant and water sides, where each refrigerant side is positioned between two water sides. In the present study, the stacked design comprises five refrigerant layers and six water layers, as illustrated in Fig. 4.

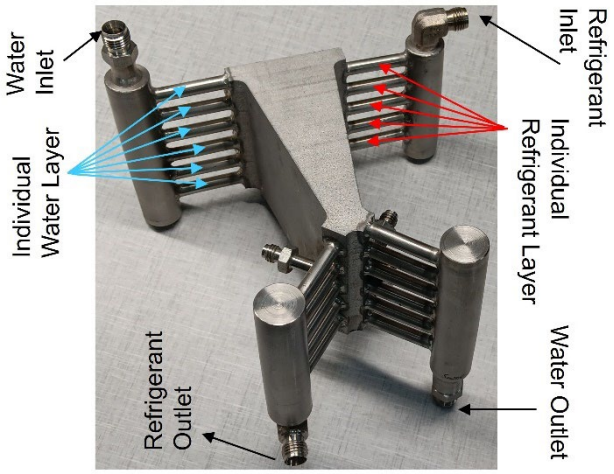

Fig. 4. Stacked condenser, including five refrigerant layers and six water layers, with the main inlet and outlet manifolds welded.

The refrigerant vapor and cold water enter their respective main inlet manifolds and then distribute through each refrigerant and water layer. The water and condensate from individual water and refrigerant layers then merge together and exit the condenser through their respective outlet manifolds. Each refrigerant and water layer has identical dimensions, similar to those of the single-layer condenser shown in Fig. 1. The overall height of the stacked condenser is 71.4 mm. The condenser was 3D printed from 17-4 PH stainless steel using the GE Concept Laser Mlab 3D printer. An in-house methanol bath was fabricated, and the condenser was continuously flushed with methanol for removal of excess powder remaining inside both refrigerant and water sides. The powder removal process was performed several times, with each process taking a sufficiently long time. After each process, water was pushed into the individual refrigerant and water sides of the condenser, and the uniformity of outflow from both sides was assessed. If the outflow was not uniform, the powder removal process was repeated until a high uniformity of outflow was achieved. Following the powder removal process, the main inlet and outlet manifolds for the water and refrigerant sides were welded to the inlet and outlet tubes, as shown in Fig. 4.

B. Two-Dimensional Gradient Pore Size Distribution Wick

The concept to develop the 2D-GPSD wick is schematically shown in Fig. 5. Each color represents a zone with a different pore size from the other zones. The pore sizes decrease from zone 1, represented in blue with the largest size, to zone 7, represented in brown with the smallest size. For the condenser in this study, the pore sizes decrease from 900 µm in zone 1 to 300 µm in zone 7, in increments of 100 µm. The X-ray image of the condenser shown in Fig. 3 illustrates 2D-GPSD wicks on the refrigerant side.

The presented condenser further improves the capillary-driven condensation beyond state-of-the-art by increasing the

capillary pressure (P_{cap}), wick permeability (μ), and effective thermal conductivity of the wick-condensate (k_{eff}), as well as delaying the flooding. The performance of a capillary-driven condensation improves through enhanced P_{cap}, μ, and k_{eff}. However, in a homogenous wick (i.e., a fixed pore size), both P_{cap} and k_{eff} are inversely related to μ, as such while small pore sizes increase P_{cap} and k_{eff}, they reduce μ. A low μ is associated with a higher viscous pressure drop of liquid inside the wick (ΔP_{wick}) and an increased risk of flooding, which degrades the condensation heat transfer. Flooding occurs when the ΔP_{wick} is greater than P_{cap}. To overcome the challenges of competing P_{cap}, k_{eff}, and μ, wicks with gradient pore size distributions have been demonstrated to partially decouple P_{cap}, k_{eff}, and μ [20,30].

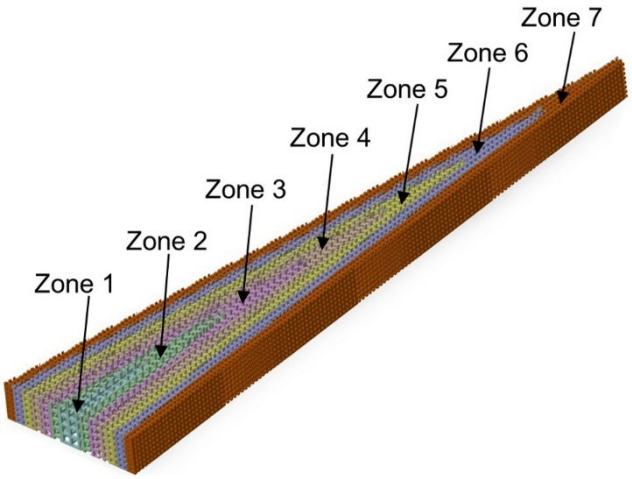

Fig. 5. Concept to illustrate the two-dimensional gradient pore size distribution (2D-GPSD) on the refrigerant side.

Additionally, the topology of the presented condenser and its capillary channels helps reduce ΔP_{wick}, which aids in preventing flooding. At a given cross-section in the capillary channel, the corresponding ΔP_{wick} for the lateral transport of liquid to each empty space is described as: $\Delta P_{\text{wick}} = (\mu_L W_{\text{eff}} \dot{m})/(\rho \mu A)$ [31], where W_{eff}, is the effective length that liquid transports laterally through the wick, μ and A are wick permeability and cross-sectional area, respectively, and $\dot{m}$, μ_L, and ρ are liquid mass flow rate, viscosity, and density, respectively. Since each capillary channel is surrounded by two empty spaces, the liquid is laterally drawn from both sides of the wick into the empty spaces. This indicates that both W_{eff} and $\dot{m}$ are split in half.

C. Flow Condensation Loop

A refrigerant flow condensation loop integrated with a water-cooled loop was fabricated for conducting flow condensation tests. Fig. 6 illustrates a simplified schematic of the test setup. Components of the individual loops were connected to each other via stainless steel tubing. The refrigerant loop was equipped with multiple heat exchangers situated before and after the condenser, Resistance Temperature Detectors (RTDs), T-type thermocouples, flowmeters, pressure transducers, control flow valves, and a positive displacement pump. The refrigerant flow rate to the condenser was adjusted using a control valve and bypass implemented after the pump and measured using a flowmeter located upstream of the condenser's inlet. The key to precise flow measurement was the use of a Coriolis (CMFS015M) flowmeter, with a range of 10 mLPM to 5 LPM. A heater was integrated into the loop and positioned before the condenser inlet to establish the thermodynamic state of the flow according to the intended specifications, such as a superheat refrigerant at the condenser inlet. The pressure at the inlet of the refrigerant side was measured using an absolute pressure transducer, and the pressure drop across the refrigerant side was measured using a differential pressure transducer (DPT). Two sight glasses, one at the inlet and another at the outlet of the refrigerant side were installed to visualize the inlet and outlet flows. The water-cooled loop was equipped with thermocouples at the inlet and outlet of the water side, a DPT to measure the pressure drop across the water side, a flowmeter, a control valve to adjust the flow rate, and a chiller to pump the water and set the temperature at the inlet of water side.

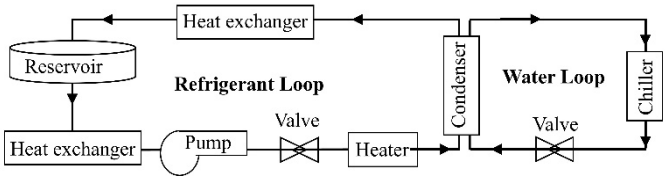

Fig. 6. Schematic of the flow condensation loop.

D. Experimental Procedure

The hermeticity of the individual refrigerant and water sides of the condenser was checked by a helium mass spectrometer with a measured leak rate less than 9×10^{-9} Std. cc/s [32]. Then, the condenser was inserted into the condensation loop. Prior to conducting the experiment, the entire loop was examined to identify any leaks before charging the loop with R134a. The liquid was circulated in the loop; then, the pump speed and the control valve were adjusted to feed the refrigerant side of the condenser with the desired flow rates. The chiller temperature on the refrigerant side was maintained at 20 °C throughout the entire experiments. By adjusting the temperature of the chiller associated with the water side, the inlet water temperature to the water side of the condenser was set. The entire condenser was covered with layers of insulation to minimize heat exchange with the ambient environment. It is possible that the outlet of the refrigerant side still has a two-phase flow. As a result, multiple heat exchangers, particularly right before the pump, were implemented to ensure that the inlet liquid to the pump is subcooled to prevent cavitation in the pump. By adjusting the voltage of the variable transformer that powered the heater, it was ensured that the inlet refrigerant to the condenser was superheat, which means no inlet refrigerant liquid entering the condenser. The superheat was determined by measuring the inlet temperature and pressure of the refrigerant and subtracting the corresponding saturation temperature at the inlet pressure from the measured inlet temperature. In the present study, all the experiments were conducted at an inlet

superheat of less than 3 °C. Tests were conducted at three different inlet water temperatures of 5 °C, 10 °C, and 15 °C, a fixed water flow rate of 3.0 LPM, and three different refrigerant flow rates of 75 mLPM, 125 mLPM, and 180 mLPM, equivalent to mass flow rates of 1.5 g/s, 2.5 g/s, and 3.5 g/s, respectively. Since the condenser comprised five refrigerant layers and six water layers, the flow rate inside each refrigerant layer is 1/5 of the total refrigerant flow rate, and the flow rate inside each water layer is 1/6 of the total water flow rate. The condenser was tested in two orientations: (i) horizontal, and (ii) vertical, with gravity aiding the condensate's exit from the bottom of the condenser. The rationale behind vertical testing is to improve the shedding process and expose condensing surfaces to incoming vapor with the assistance of gravity. Furthermore, LabVIEW was used to integrate hardware and collect signals from the RTDs, thermocouples, pressure transducers, and flowmeters in both the pumped two-phase and water loops once the system reached a steady-state condition. The steady-state condition was identified when the variations in temperatures, as measured by RTDs and T-type thermocouples remained negligible over an extended duration of system operation.

E. Data Reduction

The results are presented in terms of the condensation heat flux ($q"$) , the exit vapor quality of the refrigerant (x_e), and the pressure drop across the refrigerant side. The total cooling power provided from the water flow to the condenser ($\dot{Q}_{tot}$) is calculated as follows:

$$\dot{Q}_{tot} = \dot{m}_w\left(h_{out,w} - h_{in,w}\right) \quad (1)$$

where $\dot{m}_w$, $h_{out,w}$, and $h_{in,w}$ stand for the mass flow rate of water, outlet specific enthalpy of water, and inlet specific enthalpy of water, respectively. The $q"$ is calculated as the ratio of the $\dot{Q}_{tot}$ and the total projected area of the refrigerant side. Since each refrigerant layer is located between two water layers, condensation occurs on both sides of each refrigerant layer. Consequently, the $q"$ is calculated as follows:

$$q" = \dot{Q}_{tot}/\left(2 \times N_R \times A_{proj,R}\right) \quad (2)$$

where N_R represents the number of refrigerant layers (five in this study), and $A_{proj,R}$ denotes the projected area of each side of an individual refrigerant layer. The projected area was determined using the CAD model of the condenser.

To calculate the x_e, the specific enthalpy of the refrigerant at the outlet ($h_{out,R}$) is required, which is calculated from the energy balance, as follows:

$$h_{out,R} = h_{in,R} - \left(\dot{Q}_{tot}/\dot{m}_R\right) \quad (3)$$

where $\dot{m}_R$ is the mass flow rate of refrigerant. Then, x_e is calculated as follows:

$$x_e = \left(h_{out,R} - h_{l,R}\big|_{p,out}\right)/\left(h_{v,R}\big|_{p,out} - h_{l,R}\big|_{p,out}\right) \quad (4)$$

where $h_{v,R}\big|_{p,out}$ and $h_{l,R}\big|_{p,out}$ are the specific enthalpy values of saturated vapor and saturated liquid of the refrigerant, respectively, at the corresponding outlet refrigerant pressure.

The pressure drop across the refrigerant side of the condenser was measured using a DPT located between the main inlet and outlet of the refrigerant side.

The uncertainties of the T-type thermocouples, dimensions, flowmeters, and pressure transducers were ± 0.5 ℃, $\pm 2.54 \times 10^{-2}$ mm , $\pm 0.8\%$, and $\pm 0.08\%$, respectively. Using propagation of uncertainty analysis, the uncertainty in condensation heat flux was below 6.5%.

III. Results

The condensation tests were performed with the condenser operating in two orientations: one horizontal and the other gravity-assisted. The rationale behind the gravity-assisted orientation testing is to improve the shedding process and expose the condensing surfaces to incoming vapor with the assistance of gravity. Fig. 7 compares the $q"$ between two orientations of condenser at various refrigerant flow rates and inlet water temperatures. (H) and (G) in the figure represent the horizontal and gravity-assisted orientations, respectively.

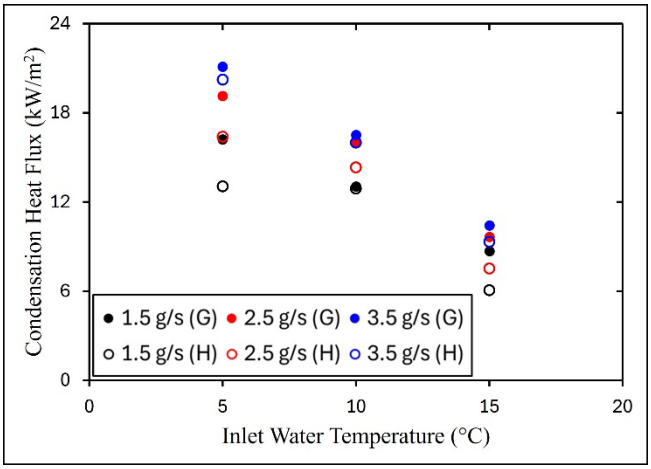

Fig. 7. Condensation heat flux for the stacked condenser at different orientations, refrigerant flow rates, and inlet water temperatures.

At a given inlet water temperature and orientation, an increase in the refrigerant flow rate results in a higher $q"$, which is attributed to the enhanced convective heat transfer occurring within the refrigerant side. At a given orientation and refrigerant flow rate, the $q"$ increases with a drop in the water inlet temperature. This is attributed to an increase in the subcooled temperature, achieved by lowering the water inlet temperature. A significant achievement is the substantial enhancement of FWC when the condenser operates in the direction of gravity as such the $q"$ increases by more than 43% at the lowest refrigerant flow rate (i.e., 1.5 g/s). As the refrigerant flow rate increases, the enhancement in $q"$ decreases, reaching over 28% at a flow rate of 2.5 g/s and over 11.7% at 3.5 g/s.

The exit vapor quality (x_e) at different refrigerant flow rates and inlet water temperatures for both condenser orientations is illustrated in Fig. 8. At a given refrigerant flow rate and

condenser orientation, the x_e decreases as the water inlet temperature decreases. This occurs because lower inlet water temperatures result in increased subcooling, thereby reducing x_e (i.e., more condensate). At the lowest refrigerant flow rate (1.5 g/s), the condenser achieved full condensation at inlet water temperatures of 5 °C and 10 °C in both horizontal and gravity-assisted orientations. Overall, due to enhanced condensation heat transfer in the gravity-assisted orientation, a lower x_e is expected compared to the horizontal operation. At the lowest refrigerant mass flow rate, aside from the first two inlet water temperatures where both orientations achieved full condensation, the gravity-assisted resulted in over 43% more condensation than the horizontal operation. At the middle refrigerant flow rate (2.5 g/s), the gravity-assisted orientation resulted in over 70%, 30%, and 16% more condensation at inlet water temperatures of 5 °C, 10 °C, and 15 °C, respectively, compared to the horizontal orientation. An important finding from Fig. 8 is the presence of a threshold refrigerant flow rate necessary for full condensation, for a given condenser design and operating conditions, such as water flow rate and inlet water temperature; for instance, 3.5 g/s is a large flow rate for the present condenser. This highlights the need for optimizing condenser features to achieve full condensation across a broader range of flow rates, which is a focus of ongoing research within our team.

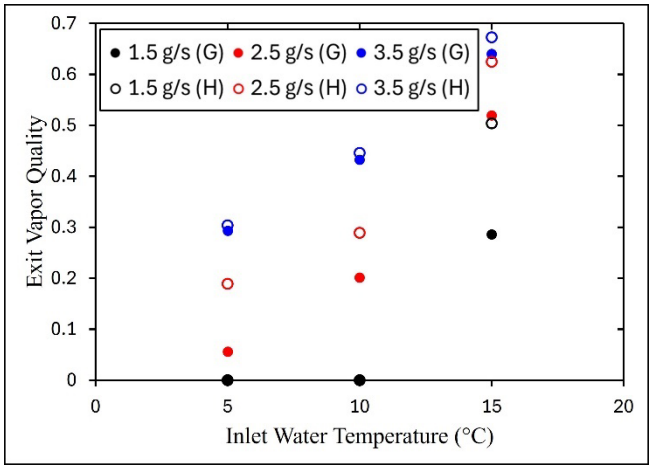

Fig. 8. Exit vapor quality at different orientations, refrigerant flow rates, and inlet water temperatures.

Fig. 9 illustrates the pressure drops across the refrigerant side of the condenser at different refrigerant flow rates and inlet water temperatures for two different condenser orientations. At a given orientation and refrigerant flow rate, the pressure drop decreases as the water inlet temperature decreases. This occurs because a lower water inlet temperature results in a lower x_e (i.e., more condensate), which in turn reduces the pressure drop. At a given orientation and inlet water temperature, increasing the flow rate raises the pressure drop due to the higher vapor velocity. Additionally, when the condenser operates in the gravity-assisted orientation, the pressure drop at a given inlet water temperature and refrigerant flow rate is higher than in horizontal testing. This is likely due to increased interaction between the vapor and condensate because with gravity assistance, more condensate is present than in horizontal operation. As observed in Fig. 9, the pressure drops at low flow rates could not be measured accurately because they were too small for the current DPT used in the experiments. For future tests, a DPT with a lower range will be used to accurately measure the pressure drops associated with low flow rates on the refrigerant side.

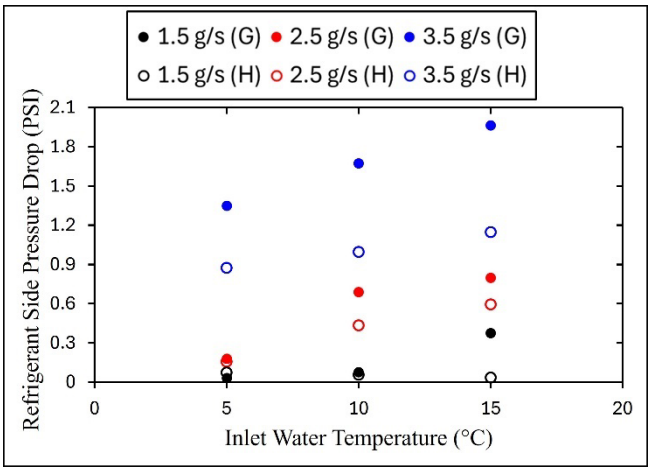

Fig. 9. Pressure drops across the refrigerant side of the condenser at different orientations, refrigerant flow rates, and inlet water temperatures.

In summary, the 3D-printed liquid-cooled condenser developed in this study demonstrated promising performance, enabling enhanced FWC of low-surface-tension fluids. Through the optimization of features on the water side, as well as the pore size distribution on the refrigerant side, further enhancement of FWC will be achieved, thereby reducing the SWaP of future thermal management hardware.

IV. Conclusion

For the first time, this study presents a scaled-up 3D-printed liquid-cooled condenser to enhance FWC of low-surface-tension fluids. The condenser comprised five refrigerant layers and six water layers, with each refrigerant layer positioned between two water layers. Water was used as the coolant to condense the vapor of refrigerant R134a. The water side featured cylindrical pin fins. The novelty of the condenser lies in the refrigerant side, which included wick structures with 2D-GPSD. The condenser was tested in two different orientations: one horizontally and the other in a gravity-assisted orientation. The results demonstrated a significant enhancement in condensation heat flux and a substantial reduction in exit vapor quality when the condenser operated in the gravity-assisted orientation compared to the horizontal orientation.

V. Future Work

Future research aimed at optimizing pore size distributions on the refrigerant side and heat transfer features on the water side is expected to further improve the hydrothermal performance of the proposed condenser, making it attractive for reducing the SWaP of future thermal management hardware.

ACKNOWLEDGMENT

The financial support from the Navy STTR, office of Naval Research, with a Contract Number N68335-23-C-0464 is gratefully acknowledged.

REFERENCES

[1] Zhou, Z.-F., Lin, X.-W., Ji, R.-J., Zhu, D.-Q., Chen, B., Wang, H., and Lu, Y.-J., "Enhancement of Heat Transfer on Micro- and Macro- Structural Surfaces in Close-Loop R410A Flashing Spray Cooling System for Heat Dissipation of High-Power Electronics," *Applied Thermal Engineering*, Vol. 223, 2023, p. 119978. https://doi.org/10.1016/j.applthermaleng.2023.119978

[2] Catuche, J., Shaeri, M. R., and Ellis, M. C., "Additive Manufacturing of Capillary-Driven Two-Phase Cold Plates," Czech Republic, Prague, 2022. https://doi.org/10.11159/htff22.174

[3] Huang, C.-N., and Kharangate, C. R., "Consolidated Model for Predicting Flow Boiling Critical Heat Flux in Single-Sided and Double-Sided Heated Rectangular Channels," *International Journal of Heat and Mass Transfer*, Vol. 160, 2020, p. 120132. https://doi.org/10.1016/j.ijheatmasstransfer.2020.120132

[4] Lei, Y., Mudawar, I., and Chen, Z., "Computational and Experimental Investigation of Condensation Flow Patterns and Heat Transfer in Parallel Rectangular Micro-Channels," *International Journal of Heat and Mass Transfer*, Vol. 149, 2020, p. 119158. https://doi.org/10.1016/j.ijheatmasstransfer.2019.119158

[5] O'Neill, L. E., Balasubramaniam, R., Nahra, H. K., Hasan, M. M., and Mudawar, I., "Flow Condensation Heat Transfer in a Smooth Tube at Different Orientations: Experimental Results and Predictive Models," *International Journal of Heat and Mass Transfer*, Vol. 140, 2019, pp. 533–563. https://doi.org/10.1016/j.ijheatmasstransfer.2019.05.103

[6] Zhou, L., Garg, D., Qiu, Y., Kim, S.-M., Mudawar, I., and Kharangate, C. R., "Machine Learning Algorithms to Predict Flow Condensation Heat Transfer Coefficient in Mini/Micro-Channel Utilizing Universal Data," *International Journal of Heat and Mass Transfer*, Vol. 162, 2020, p. 120351. https://doi.org/10.1016/j.ijheatmasstransfer.2020.120351

[7] Hu, H., Wang, Q., Chen, X., Li, Q., Du, M., and Niu, D., "Droplet Condensation and Transport Properties on Multiple Composite Surface: A Molecular Dynamics Study," *Frontiers in Heat and Mass Transfer*, Vol. 22, No. 4, 2024, pp. 1245–1259. https://doi.org/10.32604/fhmt.2024.054223

[8] Hou, Y., Yu, M., Chen, X., Wang, Z., and Yao, S., "Recurrent Filmwise and Dropwise Condensation on a Beetle Mimetic Surface," *ACS Nano*, Vol. 9, No. 1, 2015, pp. 71–81. https://doi.org/10.1021/nn505716b

[9] Mirafiori, M., Tancon, M., Bortolin, S., and Del Col, D., "Modeling of Growth and Dynamics of Droplets during Dropwise Condensation of Steam," *International Journal of Heat and Mass Transfer*, Vol. 222, 2024, p. 125109. https://doi.org/10.1016/j.ijheatmasstransfer.2023.125109

[10] Chen, Z., Modak, S., Kaviany, M., and Bonner, R., "DIRECT SIMULATIONS OF BIPHILIC-SURFACE CONDENSATION: OPTIMIZED SIZE EFFECTS," *Frontiers in Heat and Mass Transfer*, Vol. 14, 2020. https://doi.org/10.5098/hmt.14.1

[11] Ghosh, A., Beaini, S., Zhang, B. J., Ganguly, R., and Megaridis, C. M., "Enhancing Dropwise Condensation through Bioinspired Wettability Patterning," *Langmuir*, Vol. 30, No. 43, 2014, pp. 13103–13115. https://doi.org/10.1021/la5028866

[12] El Fil, B., Kini, G., and Garimella, S., "A Review of Dropwise Condensation: Theory, Modeling, Experiments, and Applications," *International Journal of Heat and Mass Transfer*, Vol. 160, 2020, p. 120172. https://doi.org/10.1016/j.ijheatmasstransfer.2020.120172

[13] Wu, S., Gao, S., Wang, H., and Deng, Z., "Dropwise Condensation Heat Transfer on Vertical Superhydrophobic Surfaces with Gradient Microgrooves in Humid Air," *International Journal of Heat and Mass Transfer*, Vol. 201, 2023, p. 123583. https://doi.org/10.1016/j.ijheatmasstransfer.2022.123583

[14] Bisetto, A., Torresin, D., Tiwari, M. K., Del Col, D., and Poulikakos, D., "Dropwise Condensation on Superhydrophobic Nanostructured Surfaces: Literature Review and Experimental Analysis," *Journal of Physics: Conference Series*, Vol. 501, 2014, p. 012028. https://doi.org/10.1088/1742-6596/501/1/012028

[15] Tancon, M., Mirafiori, M., Bortolin, S., Basso, M., Colusso, E., and Del Col, D., "Dropwise Condensation Mechanisms When Varying Vapor Velocity," *Applied Thermal Engineering*, Vol. 216, 2022, p. 119021. https://doi.org/10.1016/j.applthermaleng.2022.119021

[16] Sett, S., Yan, X., Barac, G., Bolton, L. W., and Miljkovic, N., "Lubricant-Infused Surfaces for Low-Surface-Tension Fluids: Promise versus Reality," *ACS Applied Materials & Interfaces*, Vol. 9, No. 41, 2017, pp. 36400–36408. https://doi.org/10.1021/acsami.7b10756

[17] Khalil, K., Soto, D., Farnham, T., Paxson, A., Katmis, A. U., Gleason, K., and Varanasi, K. K., "Grafted

Nanofilms Promote Dropwise Condensation of Low-Surface-Tension Fluids for High-Performance Heat Exchangers," *Joule*, Vol. 3, No. 5, 2019, pp. 1377–1388. https://doi.org/10.1016/j.joule.2019.04.009

[18] Ma, J., Sett, S., Cha, H., Yan, X., and Miljkovic, N., "Recent Developments, Challenges, and Pathways to Stable Dropwise Condensation: A Perspective," *Applied Physics Letters*, Vol. 116, No. 26, 2020, p. 260501. https://doi.org/10.1063/5.0011642

[19] Preston, D. J., Wilke, K. L., Lu, Z., Cruz, S. S., Zhao, Y., Becerra, L. L., and Wang, E. N., "Gravitationally Driven Wicking for Enhanced Condensation Heat Transfer," *Langmuir*, Vol. 34, No. 15, 2018, pp. 4658–4664. https://doi.org/10.1021/acs.langmuir.7b04203

[20] Durgam, G. V., "Capillary-Assisted Enhanced Condensation Heat Transfer for Low Surface Tension Liquids," 2018.

[21] Zheng, Y., Chen, C.-H., Pearlman, H., and Bonner, R., "Enhanced Filmwise Condensation with Thin Porous Coating," *PRTEC-14728*, 2016.

[22] Moon, H., McGregor, D. J., Miljkovic, N., and King, W. P., "Ultra-Power-Dense Heat Exchanger Development through Genetic Algorithm Design and Additive Manufacturing," *Joule*, Vol. 5, No. 11, 2021, pp. 3045–3056. https://doi.org/10.1016/j.joule.2021.08.004

[23] Xiao, Y., Wang, X., Yang, W., Yao, X., Yang, Z., Lu, Y., Wang, Z., and Chen, L., "Data-Driven Prediction of Future Melt Pool from Built Parts during Metal Additive Manufacturing," *Additive Manufacturing*, Vol. 93, 2024, p. 104438. https://doi.org/10.1016/j.addma.2024.104438

[24] Shaeri, M. R., and Demydovych, M., "3D Printed Capillary-Driven Cold Plate for Hybrid Two-Phase Cooling System," presented at the ASME 2024 Heat Transfer Summer Conference collocated with the ASME 2024 Fluids Engineering Division Summer Meeting and the ASME 2024 18th International Conference on Energy Sustainability, Anaheim, California, USA, 2024. https://doi.org/10.1115/HT2024-121704

[25] Shaeri, M. R., and Demydovych, M., "Thermal Management of Multiple High-Heat-Flux Heat Sources Using Additively Manufactured Two-Phase Cold Plate," presented at the 2024 23rd IEEE Intersociety Conference on Thermal and Thermomechanical Phenomena in Electronic Systems (ITherm), Aurora, CO, USA, 2024. https://doi.org/10.1109/ITherm55375.2024.10709620

[26] Shaeri, M. R., and Demydovych, M., "Additively Manufactured Cold Plate with Internal Phase Separator for Hybrid Two-Phase Cooling," presented at the 2024 23rd IEEE Intersociety Conference on Thermal and Thermomechanical Phenomena in Electronic Systems (ITherm), Aurora, CO, USA, 2024. https://doi.org/10.1109/ITherm55375.2024.10709435

[27] Shaeri, M. R., Bonner, R., and Catuche, J., "Additively Manufactured Hybrid Two-Phase Cold Plate," presented at the ASME 2023 International Technical Conference and Exhibition on Packaging and Integration of Electronic and Photonic Microsystems, San Diego, California, USA, 2023. https://doi.org/10.1115/IPACK2023-109991

[28] Shaeri, M. R., Demydovych, M., and Chen, C.-H., "Additively Manufactured Cold Plate Integrated With Evaporator Wicks and Phase Separators for Thermal Management of Multiple High-Heat-Flux Heat Sources," presented at the ASME 2024 International Technical Conference and Exhibition on Packaging and Integration of Electronic and Photonic Microsystems, San Jose, California, USA, 2024. https://doi.org/10.1115/IPACK2024-141775

[29] Saple, J., Ahmadi, B., Shaeri, M. R., and Bigham, S., "Experimental Study of a 3D-Printed Wick Condenser for Enhanced Condensation Heat Transfer," presented at the 2024 23rd IEEE Intersociety Conference on Thermal and Thermomechanical Phenomena in Electronic Systems (ITherm), Aurora, CO, USA, 2024. https://doi.org/10.1109/ITherm55375.2024.10709465

[30] Ahmadi, M., and Bigham, S., "Gradient Wick Channels for Enhanced Flow Boiling HTC and Delayed CHF," *International Journal of Heat and Mass Transfer*, Vol. 167, 2021, p. 120764. https://doi.org/10.1016/j.ijheatmasstransfer.2020.120764

[31] Shaeri, M. R., Bonner, R. W., and Ellis, M. C., "Thin Hybrid Capillary Two-Phase Cooling System," *International Communications in Heat and Mass Transfer*, Vol. 112, 2020, p. 104490. https://doi.org/10.1016/j.icheatmasstransfer.2020.104490

[32] Shaeri, M. R., Chen, C.-H., Bonner, R. W., and Demydovych, M., "Demonstration of CTE-Matched Two-Phase Minichannel Heat Sink," Orlando, FL, USA, 2023. https://doi.org/10.1109/ITherm55368.2023.10177605